catalysts

MDPI

Article

Tuneable Functionalization of Glass Fibre Membranes with ZnO/SnO_2 Heterostructures for Photocatalytic Water Treatment: Effect of SnO_2 Coverage Rate on the Photocatalytic Degradation of Organics

Vincent Rogé [1,*], Joffrey Didierjean [1], Jonathan Crêpellière [1], Didier Arl [1], Marc Michel [1], Ioana Fechete [2,3], Aziz Dinia [4] and Damien Lenoble [1]

1 Materials Research and Technology (MRT) Department, Luxembourg Institute of Science and Technology, 41 rue du Brill, L-4422 Belvaux, Luxembourg; joffrey.didierjean@list.lu (J.D.); jonathan.crepelliere@list.lu (J.C.); didier.arl@list.lu (D.A.); marc.michel@list.lu (M.M.); damien.lenoble@list.lu (D.L.)

2 LASMIS, Département Physique, Mécanique, Matériaux et Nanotechnologie (P2MN), Université de Technologie de Troyes (UTT)-Antenne de Nogent, 26 rue Lavoisier, 52800 Nogent, France; ioana.fechete@utt.fr

3 Institut de Chimie et Procédés Pour l'Energie, l'Environnement et la Santé (ICPEES), UMR 7515, 25 rue Becquerel, CEDEX 2, 67087 Strasbourg, France

4 Institut de Physique et Chimie des Matériaux de Strasbourg (IPCMS), UMR 7504, 23 rue du Loess, CEDEX 2, 67034 Strasbourg, France; aziz.dinia@ipcms.unistra.fr

* Correspondence: vincent.roge@list.lu; Tel.: +352-2758-88-45-55

Received: 2 June 2020; Accepted: 30 June 2020; Published: 2 July 2020

Abstract: The construction of a ZnO/SnO_2 heterostructure is considered in the literature as an efficient strategy to improve photocatalytic properties of ZnO due to an electron/hole delocalisation process. This study is dedicated to an investigation of the photocatalytic performance of ZnO/SnO_2 heterostructures directly synthesized in macroporous glass fibres membranes. Hydrothermal ZnO nanorods have been functionalized with SnO_2 using an atomic layer deposition (ALD) process. The coverage rate of SnO_2 on ZnO nanorods was precisely tailored by controlling the number of ALD cycles. We highlight here the tight control of the photocatalytic properties of the ZnO/SnO_2 structure according to the coverage rate of SnO_2 on the ZnO nanorods. We show that the highest degradation of methylene blue is obtained when a 40% coverage rate of SnO_2 is reached. Interestingly, we also demonstrate that a higher coverage rate leads to a full passivation of the photocatalyst. In addition, we highlight that 40% coverage rate of SnO_2 onto ZnO is sufficient for getting a protective layer, leading to a more stable photocatalyst in reuse.

Keywords: photocatalysis; ZnO; SnO_2; atomic layer deposition

1. Introduction

Photocatalytic water treatment has been intensively described in the last two decades. The amount of polluted water is constantly increasing, making the maintenance of reserves of clean drinkable water more and more challenging [1]. Current water depollution technologies (filtration membranes, reverse osmosis, adsorption, coagulation, deep UV with H_2O_2, etc.) have high operating costs and consume a lot of energy [2–5]. Consequently, the development of green and energy-efficient depollution technologies is attracting much attention. Photoactive materials working under sunlight are part of them. Among the different photocatalysts studied in the literature, semiconductors like ZnO or TiO_2 appear to be promising candidates as they are abundant, safe, thermally stable and display

high photocatalytic properties [6–9]. ZnO has a direct band gap of 3.2–3.3 eV at room temperature (≈380 nm) and an exciton binding energy of 60 meV, making it photoactive in the ultraviolet (UV) range. Nevertheless, the large-scale use of photocatalysis for water treatment is limited due to the fast recombination of photogenerated charge carriers in those materials.

In order to improve photocatalytic properties of ZnO, different strategies have been proposed, for example, by using doping elements to improve the photoresponse range [10,11] or developing heterostructures (heterojunctions) with other semiconductors [12,13]. Based on their band alignment, heterostructures can be classified into three types (Figure 1): type I (symmetric), type II (staggered) and type III (broken). Type I heterostructures are often found in light emitting diode (LED) systems, as they promote the recombination of photogenerated electrons/holes [14]. Type II heterostructures are particularly interesting for photocatalytic applications, since they allow the respective delocalisation of photogenerated charge carriers. Holes are driven in the valence band maximum (VBM) of one semiconductor and electrons in the conduction band minimum (CBM) of the second one [15]. Consequently, photogenerated electrons/holes' lifetimes are increased. Type III heterostructures can be applied in tunnelling field-effect transistors [16].

ZnO-based type II heterostructures can be produced using different metal oxides or metal sulphides, like TiO_2 [17], CdS [18], CdSe [19], or SnO_2 [20]. Among those, the ZnO/SnO_2 heterojunction is highly attractive for photocatalytic applications, as SnO_2 is a thermally and chemically stable material, insoluble in water, and has a band gap of 3.6 eV (≈345 nm). This is higher than that of ZnO, and thus, it is almost transparent in the 3.2–3.6 eV range. In addition, ZnO and SnO_2 have different Fermi energy levels [21] and they both possess valence bands potentials around 3.0 V/ENH and 3.8 V/ENH, respectively, i.e., higher than the $H_2O/OH^{\cdot}$ redox couple (2.8 V/ENH).

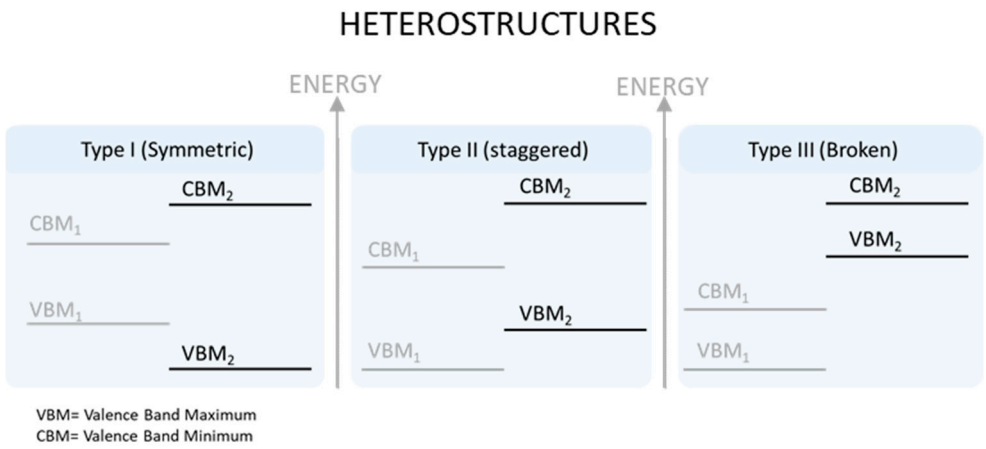

Figure 1. Schematic representation of the three different possible types of heterostructures.

According to the ZnO/SnO_2 heterostructure band alignment (Figure 2), photogenerated holes in the space charge area are delocalised in the valence band of ZnO, and electrons drift in the conduction band of SnO_2.

The synthesis of Janus-like nanoparticles, with both ZnO and SnO_2 exposed to the solution to be cleaned, is one of the most described structures in the literature [22–24]. The main advantage of such heterostructures is that holes and electrons are available for both the oxidation and the reduction of water in the form of $OH^{\cdot}$ and $O_2^{\cdot -}$ radicals, respectively. It has already been shown that $OH^{\cdot}$ radicals are the most efficient ones for water treatment [25], as they are strong oxidisers (2.8 V/ENH) able to oxidise the C–C bonds of organic molecules [26–28]. $O_2^{\cdot -}$ radicals however, follow an indirect pathway through H_2O_2 and then $OH^{\cdot}$. Therefore, the recombination rate of those radicals is higher than that of $OH^{\cdot}$ ones, and thus their photocatalytic degradation performance is usually reduced. ZnO/SnO_2 heterostructures are mostly found in the literature in the form of nanoparticles [29,30], nanorods [31] or fibres [13,32]. Various synthesis methods have been reported, such as liquid phase processes (i.e.,

sol-gel or hydrothermal growth) [33,34], electrospinning [35] or gas phase techniques [36]. However, one of the main drawbacks of this configuration is that it requires some post-treatment filtering process. As a matter of fact, a direct contact between (photo)catalytic nanoparticles and fauna and/or flora can be extremely harmful [37]. To circumvent this problem, some recent developments proposed to have the photocatalyst directly supported on a substrate [38]. Membranes are already widely used in the water treatment; coupling their physical separation properties with the photocatalytic activity of photocatalysts appears to be a promising strategy for the development of safe-by-design supported photocatalysts. This is such a strategy being pursued in the work reported here.

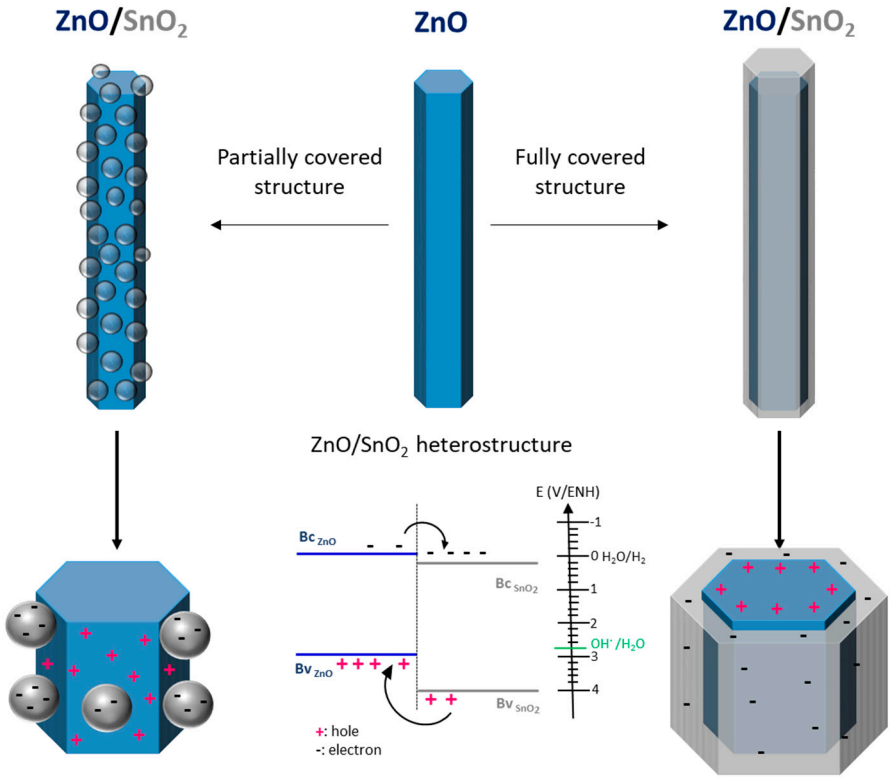

Figure 2. Schematic representation of the two possible ZnO/SnO_2 morphologies envisaged in this work. On the left, one can see that ZnO is partially covered by SnO_2 nanoparticles. In the scheme on the right, the ZnO is fully covered with a SnO_2 thin film.

In this publication, we propose to study the photocatalytic properties of ZnO/SnO_2 structures by adjusting the coverage rate of SnO_2 particles grown on ZnO nanowires. Therefore, we investigate the synthesis and characterisation of a ZnO/SnO_2 heterostructure based on ZnO nanorods/SnO_2 nanoparticles supported on glass fibres membranes. The functionalisation of glass fibres by ZnO nanorods has been performed using a liquid phase hydrothermal process and SnO_2 nanoparticles have been deposited using a gas phase Atomic Layer Deposition (ALD) process.

As presented in Figure 2, two different strategies can be foreseen to develop the desired ZnO/SnO_2 heterostructure. The first one consists in a core/shell type structure [39] obtained by a full coverage of ZnO (i.e., ZnO nanorods), with a continuous SnO_2 thin film (Figure 2, right). The advantage of this strategy is that the ZnO will be completely protected by the insoluble and stable SnO_2 film. Indeed, one of the drawbacks of ZnO is its known instability in water when the pH drops below 6 or increases above 8, unlike SnO_2, known to be stable and insoluble over a larger pH range. However, with the ZnO being completely covered by the SnO_2 thin film, photogenerated holes may be trapped inside the nanowire and not be available anymore on the surface for water oxidation ($OH^{\cdot}$ formation). In this case, only reducing species will be active for the photocatalytic degradation of contaminants via $O_2^{\cdot -}$ radical-induced reactions. The second strategy aims at partially covering ZnO nanowires with SnO_2

particles (Figure 2, left). This structure is close to a Janus one. By doing so, we expect to have a part of the ZnO surface available for photocatalytic reactions. It is yet unclear if the heterostructure formed between ZnO and SnO_2 will be efficient enough to balance the loss of ZnO exposed surface area.

As we showed in a previous work that the stability of ZnO in water could be strongly improved when protected with SnO_2, even at coverage rates below 100% [40]; the stability of the ZnO/SnO_2 over multiple reuse tests will also be studied.

2. Results and Discussion

In order to control the coverage rate of SnO_2 nanoparticles on ZnO nanorods, we used an ALD process in gas phase, with a chlorinated tin precursor. ALD deposition processes are typically used to grow conformal thin films on complex substrates. However, in some particular cases, they can be used for the synthesis of particles [41,42]. This is often attributed to the use of halogenated precursors (mainly chlorinated ones) that attack the film during the growth process, leading to particle structures [40]. This can be observed on Figure 3, where Scanning Electron Microscopy (SEM) images highlight that the growth of ZnO nanorods on each fibre of the membrane seems to be homogeneous, even on the deepest fibres. In addition, the SEM pictures point out that at a rather low number of SnO_2 ALD cycles (~500), small particles around 10 nm in size are observed on the ZnO nanorods. At 1000 cycles, the particles are slightly bigger, around 15 nm, and their density is much higher. After 1500 cycles, this effect is more pronounced, with particles around 25 nm in diameter. At 2000 cycles, ZnO nanorods seems to be almost completely covered with aggregated SnO_2 particles. Over 2500 ALD cycles, ZnO nanorods are completely covered with a granular SnO_2 film.

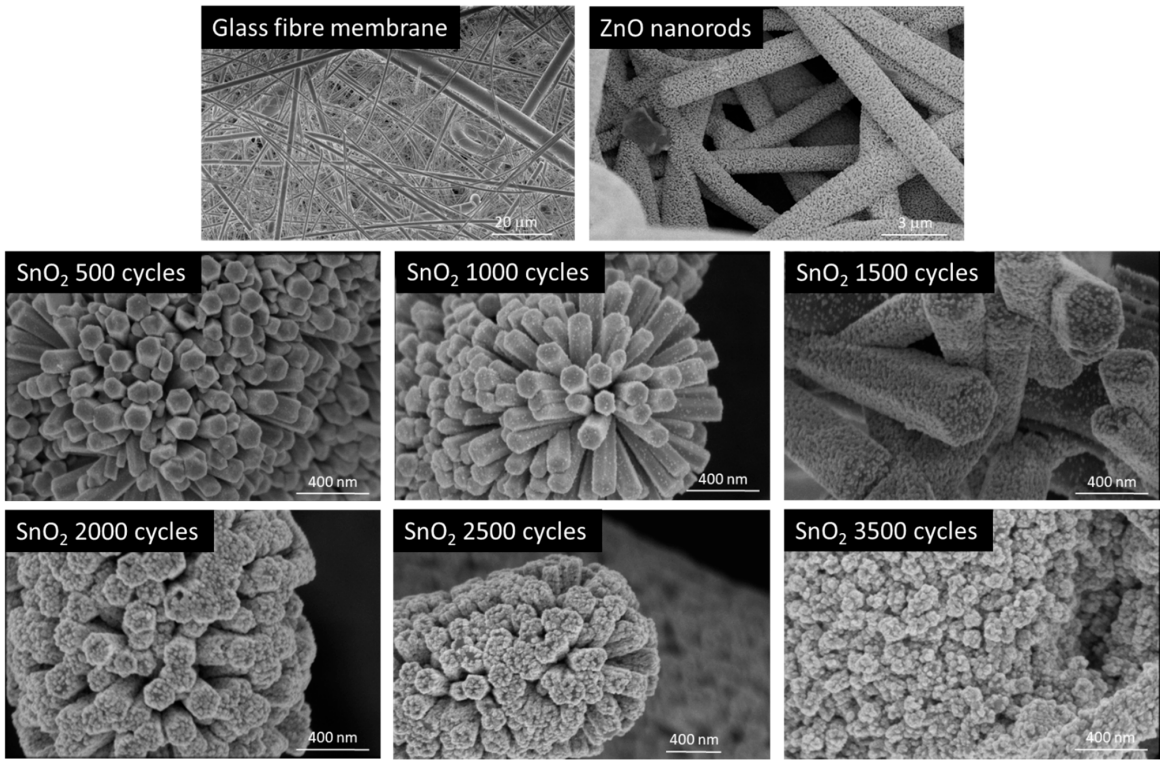

Figure 3. SEM images of a glass fibre membrane, ZnO nanorods grown in the glass fibre membrane, ZnO/SnO_2 after 500, 1000, 1500, 2000, 2500 and 3500 SnO_2 ALD cycles.

SnO_2 coverage rates have been estimated from the obtained SEM pictures using an image processing software (ImageJ software, thresholding process). A contrast is observed between SnO_2 particles and the ZnO underneath. Therefore, the image analysis is based on the roundness particles edge detection (SnO_2 particles) versus the background correction (here ZnO). Results are presented in

Figure 4. It highlights that about 8% SnO_2 coverage is achieved for 500 ALD cycles. After 1000 cycles, around 40% of the surface of nanorods is covered. A slower deposition rate is observed after 1500 cycles, with around 70% coverage. Above 2000 ALD cycles, the coverage rate is close to 100%, with some porosity due to the structure of the SnO_2 film.

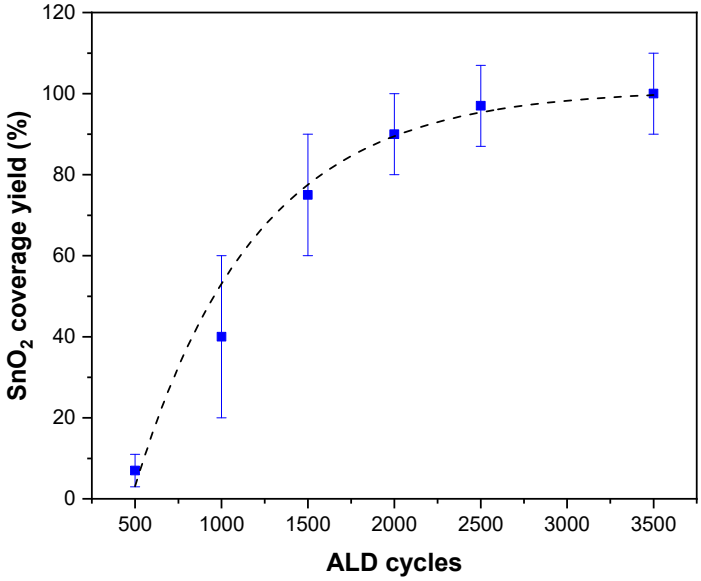

Figure 4. SnO_2 coverage rate as a function of the number of ALD cycles used (estimated from SEM pictures).

An Energy Dispersive X-ray (EDX) analysis (Figure 5a) of the synthesized ZnO/SnO_2 structure covered at 70% with SnO_2 nanoparticles reveals the presence of oxygen (Kα = 0.52 keV), Zinc (Lα = 1.01 keV, Kα1 = 8.63 keV and Kα2 = 9.53 keV), silicon (Kα = 1.74 keV) and tin (Lα = 3.44 keV and Lβ = 3.46 keV). The EDX spectrum is in accordance with the corresponding SEM picture, as we observe an intense peak of Zn related to the ZnO being the major component of the ZnO/SnO_2 structure. Peaks related to Tin are weak compared to the Zn one. This is related to the relatively small overall quantity of SnO_2 deposited on the ZnO nanowires. Indeed, the inherent volume of interaction of EDX probing down to few micrometres leads to a higher contribution of ZnO as well as the detection of silicon due to the glass fibre membrane used as support.

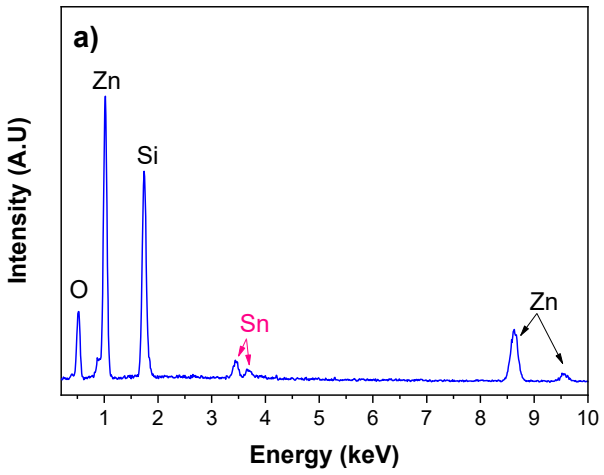

Figure 5. *Cont.*

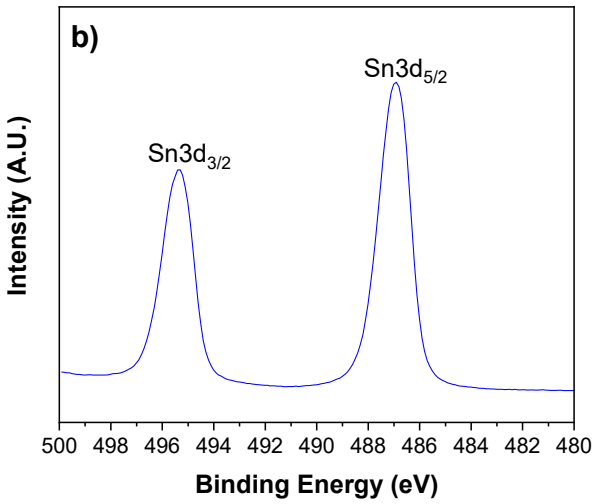

Figure 5. (**a**) EDX analysis of ZnO/SnO_2 (70% SnO_2 surface coverage). (**b**) High resolution XPS spectrum of the Sn3d peak.

Besides the first chemical screening performed by EDX analysis, an elemental composition of the developed membrane has been determined by X-ray Photoelectron Spectroscopy (XPS) analysis, with a specific focus on the oxidation state of Sn. Figure 5b corresponds to a high-resolution analysis of the Sn3d peak. In this figure, one can see the position of the $Sn3d_{3/2}$ peak at 495.4 eV and the $Sn3d_{5/2}$ peak at 486.7 eV, distinctive of a Sn^{4+} oxidised state of Sn in SnO_2 [13,43]. In addition, the coupled spin orbit splitting between the $Sn3d_{3/2}$ peak and the $Sn3d_{5/2}$ peak is exactly 8.5 eV, featuring the Sn–O bonding. The sharp shape of both peaks confirms one chemical bonding contribution: Sn–O. This further confirms that particles are composed of SnO_2.

Crystalline structures of functionalized photocatalytic membranes have been investigated by X-Ray Diffraction (XRD). Resulting diffractograms are presented in Figure 6 With a 70% SnO_2 surface coverage rate, the hexagonal wurtzite structure of ZnO is detected. The three main diffraction planes of the ZnO wurtzite structure, at 31.75°, 34.45° and 36.25°, corresponding to the (100), (002) and (101) diffraction planes, respectively, are intense and sharp. ZnO is well crystallised, which is a critical feature for efficient water treatment by photocatalysis [44]. In this sample, no SnO_2 crystalline structure can be identified. This may be due to the excessively small amount of material deposited, to the fact that the SnO_2 could have grown in an amorphous state or to very small crystallite sizes. The XRD diffractogram recorded for the sample completely covered with a SnO_2 film exhibits the same ZnO hexagonal wurtzite structure, but weak diffraction peaks characteristic of the tetragonal cassiterite structure of SnO_2 are also visible. They correspond to the (100), (101) and (211) diffraction planes at 26.54°, 33.89° and 51.78° respectively. The presence of those peaks confirms that the SnO_2 is crystalline. Nevertheless, the relative amount deposited compared to ZnO is too low to see some intense and well-defined peaks. Considering the configuration of the ZnO/SnO_2 heterostructure grown in a glass fibre membrane (with circular fibres), the probing of the surface with a grazing angle XRD analysis in very challenging to set up and not fully representative of the global structure.

Crystalline ZnO has a direct optical and electronic band gap of approximately 3.2 eV. It absorbs UV light and show photoluminescent properties with a near band edge (NBE) emission around 380 nm (3.2 eV), corresponding to the excitonic radiative recombination. This emission band is usually sharp and intense for highly crystalline ZnO materials. A second band is often observed in the visible region, centred in the green zone around 530 nm (2.33 eV), corresponding to deep level emission (DLE), due to defects in the ZnO matrix [45,46].

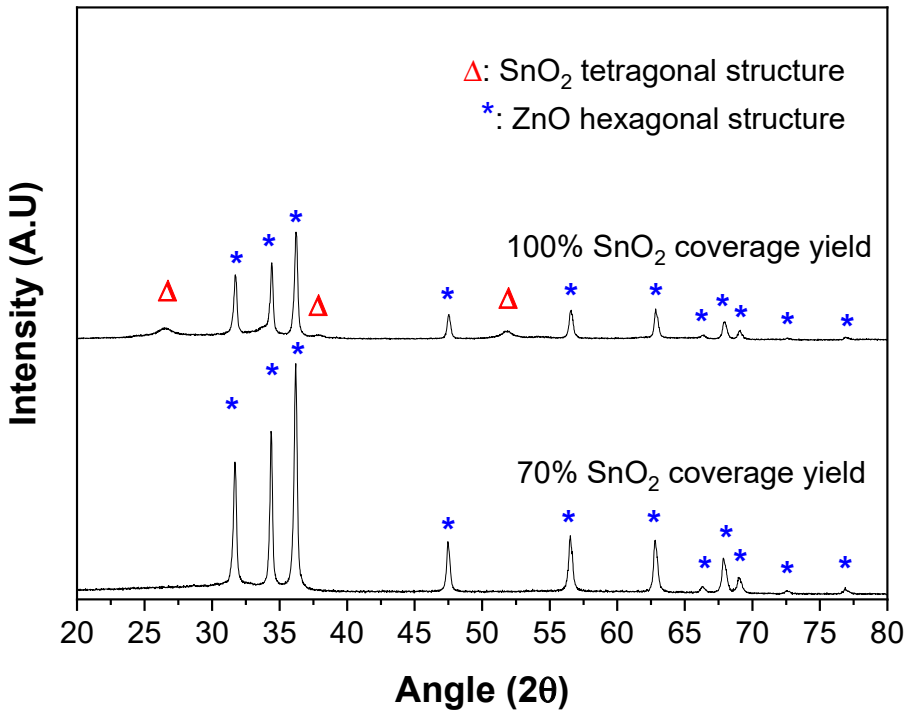

Figure 6. XRD diffractograms of the ZnO/SnO_2 heterostructure synthesized in glass fibre membranes after different SnO_2 coverage rate.

The optical properties of the synthesized ZnO nanorods and ZnO/SnO_2 structures after 70% and 100% coverage rate are presented in Figure 7. An intense and sharp peak is observed at 384 nm for ZnO nanorods. The emission peak related to defects in this case is relatively weak. This suggests that ZnO nanorods are highly crystalline with low defects, further reinforcing the conclusion drawn from the XRD analysis.

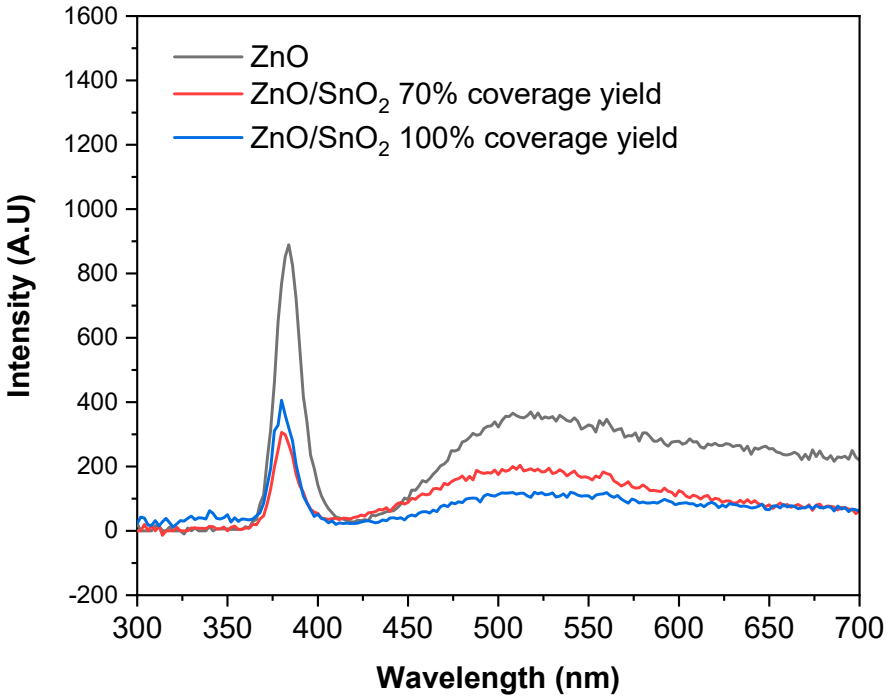

Figure 7. Photoluminescence spectra of ZnO nanorods, ZnO/SnO_2 with 70% coverage rate and ZnO/SnO_2 with 100% coverage rate.

When ZnO nanorods are covered by SnO_2, partially or totally (70% or 100%), the NBE emission is lowered in intensity, but still present. This lowering of intensity can be assigned to the presence of the heterostructure between ZnO and SnO_2, which stabilises photogenerated carriers, and thus, limits the radiative recombination and consequently the NBE emission intensity. Interestingly, the NBE emission intensity is in the same order of magnitude for the ZnO covered at 70% by SnO_2 and for the ZnO fully covered by SnO_2.

This reveals two important features when considering photocatalytic applications. Firstly, SnO_2 remains transparent to UV light, so that the ZnO underneath can still be excited, generating electron/hole carriers, even when fully covered. Secondly, a 70% coverage rate of SnO_2 is enough to prevent charge carriers recombination. The presence of the broad peak in the visible range can be attributed to remaining defects in the ZnO or SnO_2, particularly oxygen vacancies. The annealing treatment of ZnO, as well as the growth temperature of SnO_2, were limited to 300 °C because of the substrate instability above this temperature. Thus, it is likely that all oxygen vacancies were not completely eliminated [47,48].

The photocatalytic degradation properties of ZnO/SnO_2 structures have been investigated with standard methylene blue (MB). MB is a well-known and widely used chemical probe for the simple investigation of photocatalytic efficiencies of metal oxide photocatalysts. Five samples have been tested: ZnO nanorods without SnO_2, ZnO/SnO_2 with 8% coverage rate, ZnO/SnO_2 with 40% coverage rate, ZnO/SnO_2 with 70% coverage rate and ZnO/SnO_2 with 100% coverage rate. Results are presented in Figure 8.

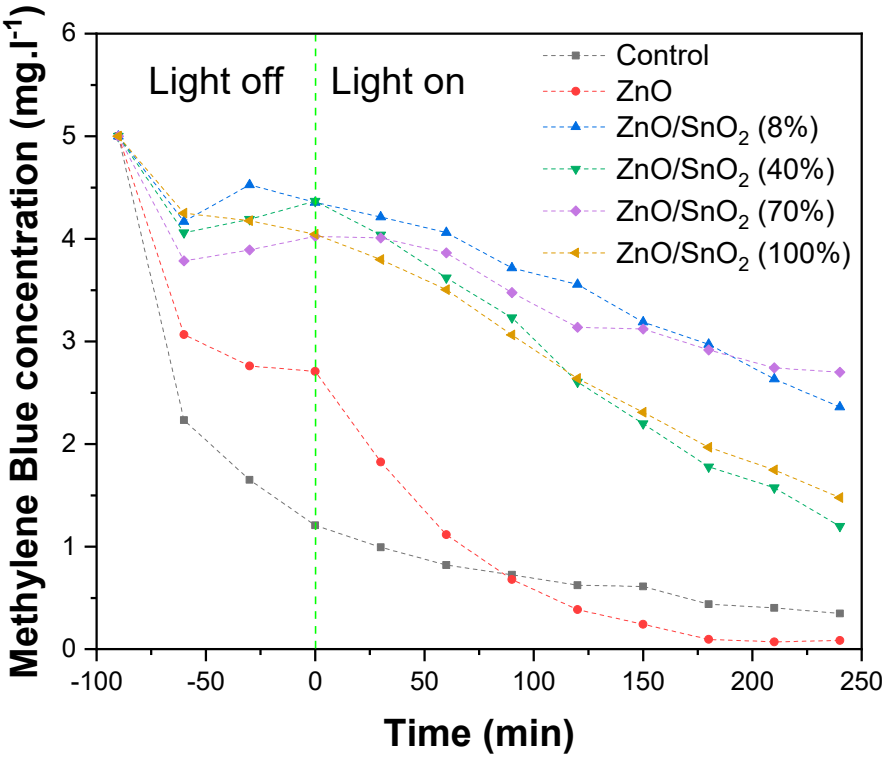

Figure 8. Photocatalytic degradation of Methylene blue under UV light (365 nm, 8 W) over ZnO or ZnO/SnO_2 photocatalysts. Percentages in bracket indicate the coverage rate of SnO_2 nanoparticles around ZnO.

In a first step, membranes were exposed to the solution in the dark for 90 min in order to stabilise the adsorption/desorption of MB on membranes. This process is crucial for a reliable determination of the photocatalytic degradation kinetics. If not taken into account, this may induce errors due to the uncertainty of distinguishing between adsorption and degradation phenomena. The control

membrane (glass fibre only without any photocatalyst) showed high adsorption properties of the organic methylene Blue in the dark, as the measured concentration in solution decreased drastically from 5 $mg{\cdot}L^{-1}$ down to 1 $mg{\cdot}L^{-1}$. The membrane functionalized with ZnO nanorods also showed good adsorption properties toward MB, but less than glass fibres, as the concentration dropped from 5 $mg{\cdot}L^{-1}$ down to 2.7 $mg{\cdot}L^{-1}$. ZnO/SnO_2 heterostructure-based membranes exhibited lower affinity for MB, as less than 1 $mg{\cdot}L^{-1}$ was adsorbed (5 $mg{\cdot}L^{-1}$ down to more than 4 $mg{\cdot}L^{-1}$), independently of the coverage rate. UV light irradiation on the control membrane (which corresponds to t = 0) had no visible effect on its behaviour toward MB. The picture in Figure 9 confirms that the MB is just adsorbed on the glass fibres, and not degraded. Indeed, the control membrane on the left-hand side of Figure 9 is completely blue after the photocatalytic test, which is not the case of the ZnO/SnO_2 photocatalytic membrane on the right-hand side of the picture. The ZnO functionalised membrane showed a peculiar behaviour compared to the control after exposure to UV light. A decrease in the MB concentration following pseudo first order kinetics can be observed. In less than 200 min, the solution has been completely decoloured. Surprisingly, all ZnO/SnO_2 membranes revealed very low photocatalytic properties, independently from the SnO_2 coverage rate. The adsorption process in the dark revealed a poor affinity with all surfaces, which could explain the slow degradation of MB. Another hypothesis could be that impurities trapped in the film or at the surface may act as scavengers for photogenerated carriers (e^-/h^+) or photogenerated OH· radicals. Considering the growth process of SnO_2 with the chlorinated precursor $SnCl_4$, chlorine could be present in/on the ZnO/SnO_2 structure and strongly affect the resulting photocatalytic properties [49]. In order to investigate the role of surface defects or residual chlorine, a model structure has been prepared by growing a ZnO/SnO_2 thin film on a silicon wafer, covered with 2–3 nm native oxide. Depth profiling of the sample was performed by Secondary Ions Mass Spectrometry (SIMS) analysis.

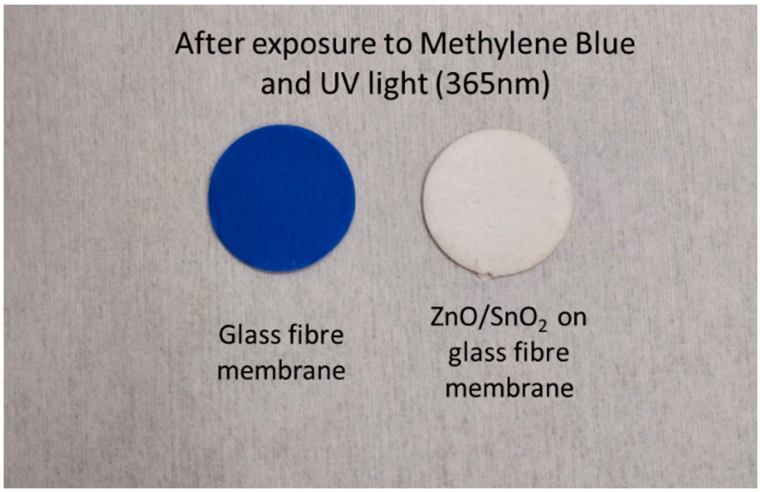

Figure 9. Picture of a glass fibre membrane after exposure to methylene blue (left) and glass fibre membrane functionalised with ZnO nanorods/SnO_2 (70% coverage rate) (right).

Figure 10 presents the uncalibrated concentration vs. depth of five elements tracked during the SIMS analysis: silicon, tin, zinc, chlorine and oxygen. The stack SnO_2/ZnO is featured by a high contribution of tin in the first 400 s of pulverisation followed by the zinc contribution from 500 to 1200 s. The oxygen contribution remains stable along the depth profile (pulverisation time from 0 s to 1200 s). After 1200 s of pulverisation, the zinc and oxygen contributions disappear in favour of silicon corresponding to the substrate contribution. Interestingly, a high contribution of chlorine is detected in the SnO_2 film. When the ZnO film is formed, the contribution of chlorine is lowered drastically. However, some chlorine is still visible in the ZnO film. This clearly evidences the fact that Cl is trapped within the SnO_2 films during its growth and that it slightly diffuses into the ZnO underneath. No chlorine is detected in the substrate level.

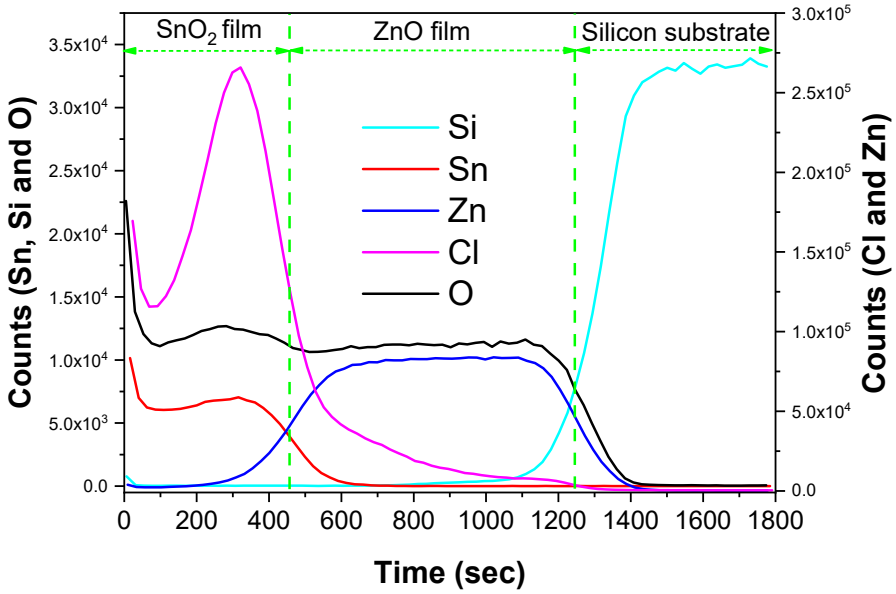

Figure 10. Depth profile SIMS analysis of SnO_2 grown by ALD on ZnO (a mirror-polished silicon wafer was used as substrate).

In order to remove defects like oxygen vacancies or chlorine, as-prepared ZnO/SnO_2 membranes have been cleaned under a UV/ozone atmosphere (254 nm, 20 W) for 30 min. Compared to plasma or thermal post-treatments, the dry UV/ozone (also called UVO, for ultra-violet ozone) post-treatment has been favoured for its ability to generate, at room temperature, clean and well-oxidised metal oxide structures with very low impact on their morphologies [50]. Also, this technique is known for being able to effectively remove chlorine defects from SnO_2 structures [51]. Photocatalytic degradation tests of MB have been performed again. They are presented on Figure 11.

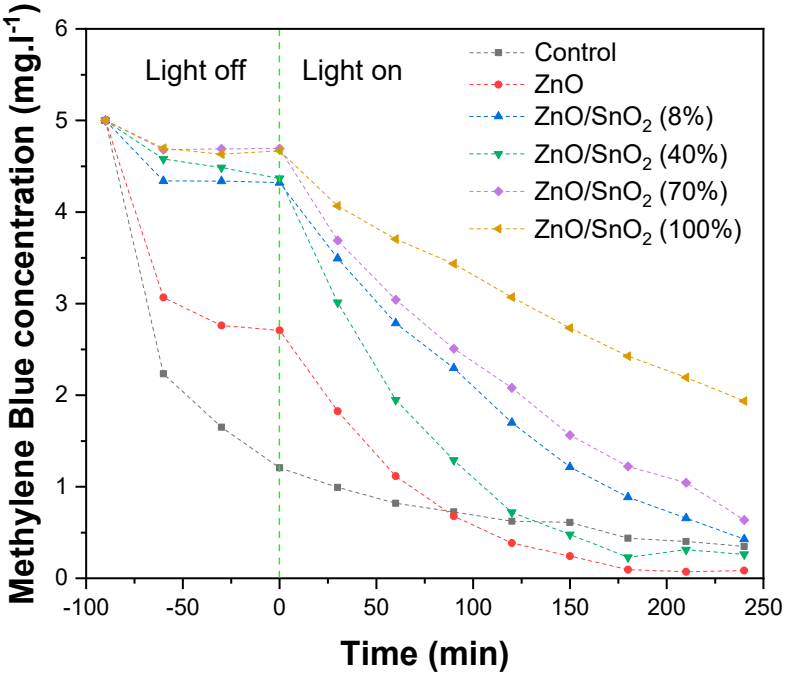

Figure 11. Photocatalytic degradation of methylene blue under UV light (365 nm, 8 W) over ZnO or ZnO/SnO_2 photocatalysts after UV/ozone treatment. Percentages in brackets indicate the coverage rate of SnO_2 nanoparticles around ZnO.

After cleaning, the affinity with the surface in the dark is not enhanced, but the photocatalytic degradation properties under UV light have been greatly improved for ZnO/SnO_2 heterostructures with 8%, 40% and 70% coverage rates. Among them, the heterostructure with 40% coverage rate is the quickest at cleaning the solution of MB according to the steep slope (starting from t = 0). Concerning the ZnO/SnO_2 heterostructure with 100% coverage rate, the cleaning had absolutely no impact on its poor photocatalytic degradation properties. The disappearance of MB remains slow compared to other synthesized heterostructures.

The photocatalytic degradation of MB over ZnO and ZnO/SnO_2 photocatalysts seems to follow pseudo-first order degradation kinetics, as usually observed when considering the photocatalytic degradation of pollutants in water [52,53]. Consequently, from the results obtained on Figure 8 (before cleaning) and Figure 11 (after cleaning), we determined the first order degradation rate constant k (in min^{-1}) of the photocatalysts by using the following equation:

$$\frac{C_0}{C} = e^{kt} \quad (1)$$

where C_0 is the initial concentration after 90 min in dark ($mg{\cdot}L^{-1}$), C the concentration ($mg{\cdot}L^{-1}$) at the time t (min). Calculated k, extracted from a plot of $\ln(C_0/C)$ versus t, are reported on Figure 12.

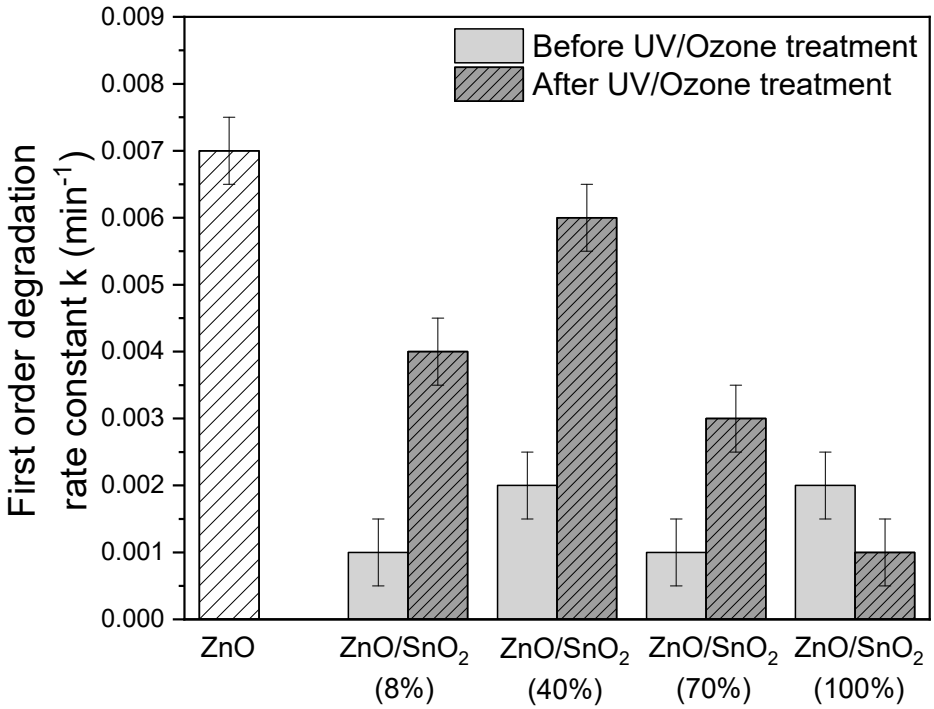

Figure 12. First order degradation rate constant k (min^{-1}) of ZnO and ZnO/SnO_2 photocatalysts before and after UV/Ozone cleaning.

The first order degradation rate constant of ZnO nanorods is found to be 7×10^{-3} min^{-1}. When covered by SnO_2 (even partially) without any cleaning, the rate drops to $1 \times 10^{-3} - 2 \times 10^{-3}$ min^{-1} for all samples. Chlorine defects seems to inhibit completely the photocatalytic activity of the material. However, after cleaning, degradation rates increased from 1×10^{-3} min^{-1} up to 4×10^{-3} min^{-1} for the ZnO/SnO_2 heterostructure with 8% SnO_2 coverage rate, 2×10^{-3} min^{-1} up to 6×10^{-3} min^{-1} for 40% SnO_2 coverage rate, 1×10^{-3} min^{-1} up to 3×10^{-3} min^{-1} for 70% SnO_2 coverage rate. With 100% SnO_2 coverage rate, however, no significant improvement is observed. Those results highlight an optimum coverage rate of ZnO by SnO_2 of around 40%, with a maximum rate value obtained of 6×10^{-3} min^{-1}. As discussed above in Figure 2, a trade-off exists between the ZnO surface

availability for the photocatalytic degradation and the number of SnO_2 nanoparticles available at the surface for the heterostructure-based stabilisation of charge carriers. In the case of a very low SnO_2 nanoparticle coverage (8%), the loss of specific surface area of ZnO free for the photodegradation is more impactful than the presence of the heterostructure. For a coverage of 70% and beyond, the heterostructure delocalises the photogenerated holes in the core of the nanorod and inhibits the photocatalytic performance of the material. Around 40% coverage, the loss of specific surface area is compensated by the effect of the heterostructure on the surface. The ZnO/SnO_2 heterostructure developed at 40% coverage rate shows a photocatalytic efficiency close that of ZnO alone. Although this is not a strong improvement, it is still interesting as the SnO_2 acts as a protective coating, preventing the dissolution of ZnO in water, even when not completely covering the surface. We demonstrated this tendency in a previous work [40], where SnO_2 protected ZnO inside mesoporous anodic aluminium oxide membranes.

In the present case, we highlight the same protective behaviour of the ZnO/SnO_2 heterostructure through reusability photocatalytic tests and SEM pictures. In Figure 13, the reusability of both ZnO (a) and ZnO/SnO_2 (40%) (b) membranes after five photocatalytic degradation tests is presented. For both systems, the photocatalytic performance is slightly improved after several reuse tests. The reason for this improvement is not yet known, but it is likely that after exposure to UV for several hours, membranes surfaces get cleaner (degradation/removal of adsorbed surface carbon) and thus more reactive toward MB. Those reusability tests demonstrate the excellent performance of ZnO and ZnO/SnO_2 membranes for water depollution over time.

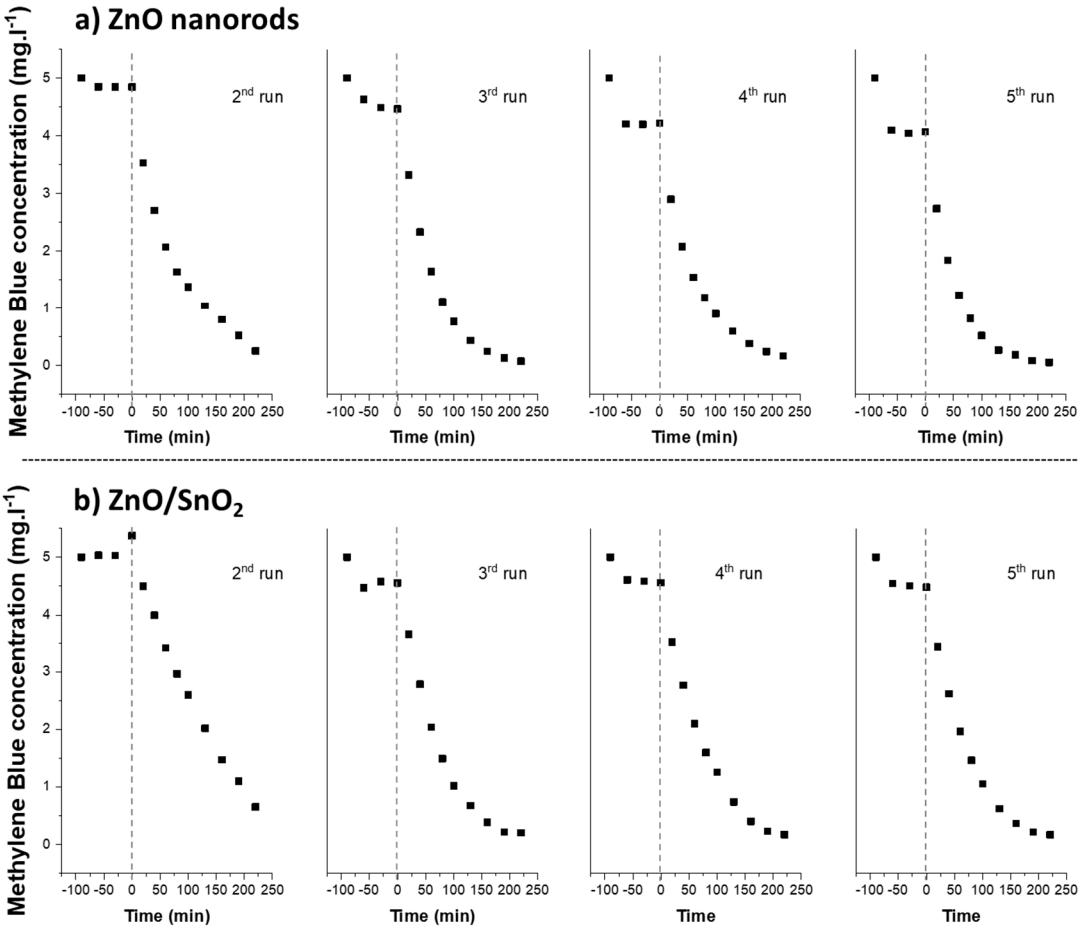

Figure 13. Reusability of ZnO (**a**) and ZnO/SnO_2 (40%) (**b**) functionalized membranes. Five photocatalytic tests have been performed.

If the excellent stability of the two membranes has been determined over five successive tests, the surface state of ZnO and ZnO/SnO_2 after those reusability tests is really different. Figure 14 presents SEM images for both ZnO and ZnO/SnO_2 functionalized membranes after the five photocatalytic degradation tests. On Figure 14a, we can clearly see that the ZnO nanorod structure has been damaged. On some glass fibres, the ZnO nanorods have completely disappeared. The remaining ZnO nanorods are shorter in length and diameter than before photocatalysis. In addition, an organic matrix, most likely some remaining traces of methylene blue, is present on their surface. This indicates an incomplete degradation of the pollutant. This hypothesis is confirmed by the presence of an intense carbon peak on the EDX spectrum (no carbon was detected before the photocatalytic degradation tests). In the case of the ZnO/SnO_2 heterostructure with 40% SnO_2 coverage rate (Figure 14b), the morphology of the photocatalyst is the same after five runs as before. The ZnO nanorods are undamaged and SnO_2 nanoparticles at the surface are still visible. Moreover, the surface seems to be clean, without any organic traces. The EDX analysis of the photocatalyst confirms that no carbon is detected on the surface. In addition, the peak related to the tin element attests to the presence of SnO_2 nanoparticles on the surface of the photocatalyst. Those results clearly highlight that over several degradation cycles, the ZnO photocatalytic properties will inexorably be lowered. Conversely, the ZnO/SnO_2 membrane appears to be more stable as a function of the degradation time. We demonstrate here the huge potential of the heterostructure, both as an efficient photoactive material and a stable heterojunction, due to the protective role of the SnO_2 around the ZnO.

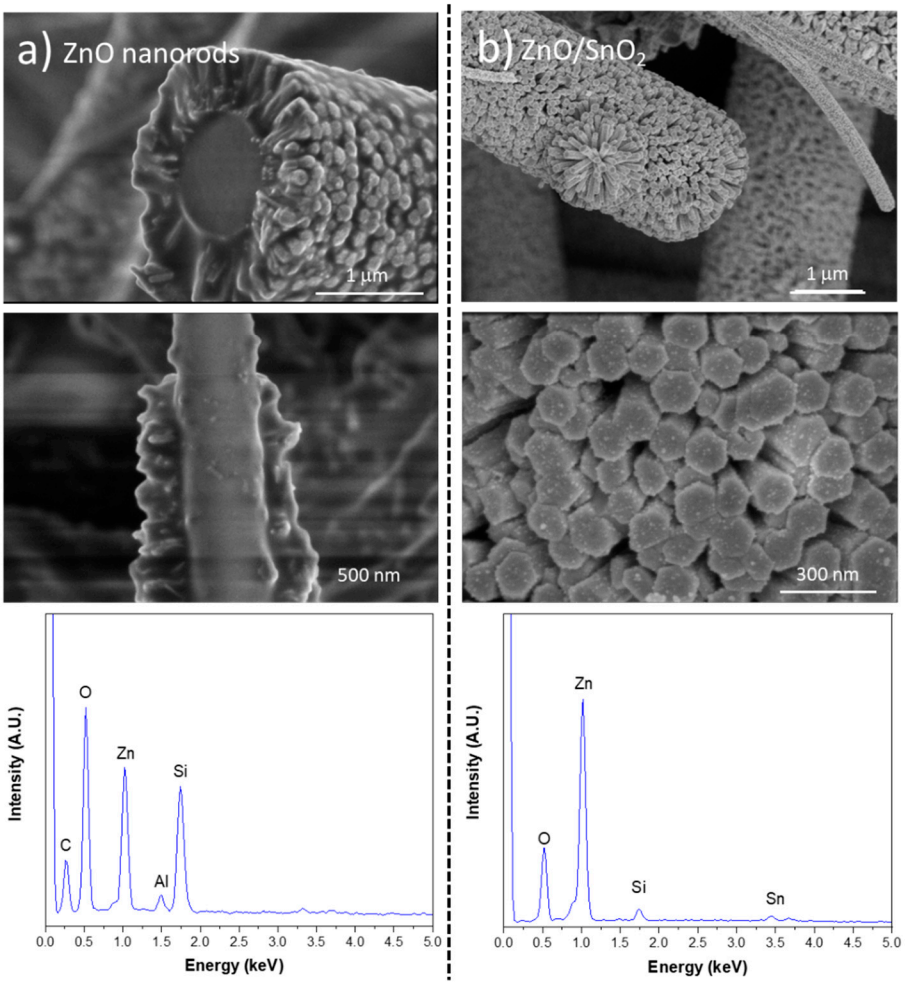

Figure 14. SEM images and EDX analysis of (**a**) ZnO nanorods and (**b**) ZnO/SnO_2 (40%) heterostructure, after five photocatalytic degradation tests.

3. Experimental Section

3.1. Materials and Experimental Processes

All chemicals were purchased from Sigma Aldrich (St. Louis, Missouri, United States), and used as received. Glass fibres membranes (APFB, 1 µm pore, 25 mm diameter without binder) were provided by Merck Millipore (Darmstadt, Germany). ZnO nanorods were synthesized in liquid phase by using zinc acetate (99.999%) and 98% anhydrous hydrazine in ultrapure water. Typically, a 25 mM zinc acetate solution was prepared with ultra-pure water in a flask equipped with a reflux system. Then, 25 mM of anhydrous hydrazine was added under vigorous steering (400 rpm). After homogenisation, the glass fibre membrane was dipped in the solution using a home-made holder. The reaction temperature was set to 80 °C for 2 h, under stirring and reflux. At the end of the reaction, the membrane was cleaned in ultra-pure water, dried, and annealed at 300 °C under an air atmosphere. The annealing process allows for the elimination of defects in the ZnO and enhances the crystallinity of ZnO rods, leading to a photocatalytic performant material. The SnO_2 growth on ZnO nanorods has been achieved by a gas phase ALD process, in a TFS200 instrument (BENEQ®, Espoo, Finland). Tin (IV) chloride ($SnCl_4$) precursor was used as the tin source and water as the oxidant. Precursors were stored at room temperature and low pressure in canisters. All precursors were introduced into the reaction chamber without any carrier gas. The reaction was performed between 1 to 5 mbar with nitrogen as carrier and purging gas. The chamber temperature was set at 300 °C during the reaction. A repeated number of $SnCl_4$/purge/H_2O/purge cycles allowed the control of the coverage rate of SnO_2 around ZnO nanorods. A typical ALD cycle can be described as follows (based on preliminary studies not shown here): 300 ms pulse of $SnCl_4$/2 s purge with nitrogen/300 ms pulse of H_2O/2 s purge with nitrogen. The number of cycles has been fixed between 500 and 3500 in order to investigate different SnO_2 particle densities, defined as coverage rate.

3.2. Characterisation Techniques

High-resolution Scanning Electron Microscopy (SEM) images were obtained on a Helios Nanolab 650 microscope (FEI, Eindhoven, The Netherlands), at an acceleration voltage of 2 kV and a current of 25 mA. Energy Dispersive X-ray (EDX) analyses were performed with a 50 mm^2 Xmax spectrometer (Oxford Instruments, Abington, UK), connected to a Helios Nanolab SEM. The working acceleration voltage was set to 10 kV for a current of 50 mA. XPS analyses were fulfilled with an Axis Ultra DLD X-ray spectrometer from Kratos Analytical (Manchester, UK), working with an Al Kα X-ray source (λ = 0.8343 nm, hυ = 1486,6 eV) at 150 W. The crystallographic structures of ZnO/SnO_2 photocatalysts were studied by X-ray diffraction (XRD) in a Brüker D8 (Billerica, MA, USA) Discover diffractometer, with a Cu Kα X-ray source (λ = 0.1542 nm) in θ-2θ mode. The photoluminescent properties of ZnO/SnO_2 were determined with an Infinite M1000 pro spectrometer (TECAN, Männedorf, Switzerland), at an excitation wavelength of 280 nm and a detection range from 300 nm to 700 nm. The secondary ion mass spectrometry (SIMS) technique has been used to determine the different elements present in the photocatalysts. Experiments were performed in a SC Ultra system (CAMECA, Gennevilliers, France), with Cs ions accelerated at an energy of 1 keV. To perform this analysis, the ZnO/SnO_2 structure (20 nm thick SnO_2 film on 50 nm thick ZnO) has been grown on (100) one side polished silicon wafers covered with a 2–3 nm native oxide layer.

3.3. Photocatalytic Degradation of Methylene Blue

The photocatalytic characterisation of ZnO/SnO_2 heterostructures on methylene blue (MB) was carried out in 6-well plates (from Greiner, Kremsmünster, Austria, 35 mm well diameter, 2 mm height, 15 mL maximum volume), with 5 mL of a solution of MB at 5 $mg{\cdot}L^{-1}$, under homogeneous stirring. The samples to be analysed were placed in separated wells. Like in many publications dealing with photocatalytic materials' performances, methylene blue has been used as a chemical probe to determine the degradation kinetic induced by different ZnO/SnO_2 photocatalysts [54–56]. MB concentration

during the photocatalytic degradation process was determined from optical absorption measurements at 666 nm using the TECAN Infinite M1000UV-visible spectrometer. Photocatalysts were irradiated with a tubular UV lamp (from Hitachi, Chiyoda City, Tokyo, Japan, F8T5, 8 W) working at 365 nm, with a measured power density of 2.28 $mW \cdot cm^{-2}$.

4. Conclusions

ZnO/SnO_2 heterostructures have been synthesised in macroporous glass fibres membranes using a hydrothermal process to grow ZnO nanorods along with a gas phase ALD process for the SnO_2 growth. We show that by adjusting the number of ALD cycles, it is possible to synthesize SnO_2 particles with a fine control of the coverage rate. Those functionalised membranes have been tested for the photocatalytic degradation of methylene blue under UV light. It has been shown that an optimum coverage rate of approximately 40% led to the most efficient photocatalytic activity against MB. Indeed, it appeared that the exposure of the ZnO surface to the solution to be cleaned is an important parameter for efficient photocatalysts, and that higher coverage rates inhibit the ZnO/SnO_2 structures' activity. We also point out that the ZnO/SnO_2 heterostructure with 40% coverage rate was highly stable in water after many reuse tests, whereas ZnO nanorods alone were damaged.

Author Contributions: Conceptualization, V.R., D.A., M.M., I.F., D.L.; methodology, V.R., J.D., J.C.; validation, I.F., A.D., D.L.; formal analysis, V.R., J.D., J.C.; writing—original draft preparation, V.R., J.D., J.C., D.A., M.M., I.F., A.D., D.L.; supervision, I.F., A.D., D.L.; project administration, M.M., D.A., D.L.; funding acquisition, D.L. All authors have read and agreed to the published version of the manuscript.

Funding: This research was funded by the "Fond National de la Recherche Luxembourgeoise" (FNR) on the NaneauII project (2015, project number C10/SR/799842).

Conflicts of Interest: The authors declare no conflict of interest.

References

1. Boretti, A.; Rosa, L. Reassessing the projections of the World Water Development Report. *NPJ Clean Water* **2019**, *2*, 1–6. [CrossRef]
2. Sharma, S.; Bhattacharya, A. Drinking water contamination and treatment techniques. *Appl. Water Sci.* **2016**, *7*, 1043–1067. [CrossRef]
3. Macedonio, F.; Drioli, E. Membrane Engineering for Green Process Engineering. *Engineering* **2017**, *3*, 290–298. [CrossRef]
4. Wünsch, R.; Plattner, J.; Cayon, D.; Eugster, F.; Gebhardt, J.; Wülser, R.; Von Gunten, U.; Wintgens, T. Surface water treatment by UV/H2O2 with subsequent soil aquifer treatment: Impact on micropollutants, dissolved organic matter and biological activity. *Environ. Sci. Water Res. Technol.* **2019**, *5*, 1709–1722. [CrossRef]
5. Epimakhov, V.N.; Oleinik, M.S.; Moskvin, L.N. Reverse-Osmosis Filtration Based Water Treatment and Special Water Purification for Nuclear Power Systems. *At. Energy* **2004**, *96*, 234–240. [CrossRef]
6. Fu, D.; Han, G.; Meng, C. Size-controlled synthesis and photocatalytic degradation properties of nano-sized ZnO nanorods. *Mater. Lett.* **2012**, *72*, 53–56. [CrossRef]
7. Kahng, S.; Yoo, H.; Kim, J.H. Recent advances in earth-abundant photocatalyst materials for solar H2 production. *Adv. Powder Technol.* **2020**, *31*, 11–28. [CrossRef]
8. Ishchenko, O.M.; Rogé, V.; Lamblin, G.; Lenoble, D. TiO_2- and ZnO-Based Materials for Photocatalysis: Material Properties, Device Architecture and Emerging Concepts. In *Semiconductor Photocatalysis—Materials, Mechanisms and Applications*; IntechOpen: London, UK, 2016. [CrossRef]
9. Rogé, V.; Guignard, C.; Lamblin, G.; Laporte, F.; Fechete, I.; Garin, F.; Dinia, A.; Lenoble, D. Photocatalytic degradation behavior of multiple xenobiotics using MOCVD synthesized ZnO nanowires. *Catal. Today* **2018**, *306*, 215–222. [CrossRef]
10. Chang, C.-J.; Lin, C.-Y.; Hsu, M.-H. Enhanced photocatalytic activity of Ce-doped ZnO nanorods under UV and visible light. *J. Taiwan Inst. Chem. Eng.* **2014**, *45*, 1954–1963. [CrossRef]
11. Lavand, A.B.; Malghe, Y.S. Synthesis, Characterization, and Visible Light Photocatalytic Activity of Nanosized Carbon Doped Zinc Oxide. *Int. J. Photochem.* **2015**, *2015*, 1–9. [CrossRef]

12. Belver, C.; Hinojosa-Reyes, L.; Bedia, J.; Tobajas, M.; Alvarez, M.A.; Rodríguez-González, V.; Rodriguez, J.J. Ag-Coated Heterostructures of ZnO-TiO_2/Delaminated Montmorillonite as Solar Photocatalysts. *Materials* **2017**, *10*, 960. [CrossRef]
13. Zhang, Z.; Shao, C.; Li, X.; Zhang, L.; Xue, H.; Wang, C.; Liu, Y. Electrospun Nanofibers of ZnO–SnO_2 Heterojunction with High Photocatalytic Activity. *J. Phys. Chem. C* **2010**, *114*, 7920–7925. [CrossRef]
14. Wang, S.; Tian, H.; Ren, C.; Yu, J.; Sun, M. Electronic and optical properties of heterostructures based on transition metal dichalcogenides and graphene-like zinc oxide. *Sci. Rep.* **2018**, *8*, 12009. [CrossRef]
15. Hu, W.; Yang, J. Two-dimensional van der Waals heterojunctions for functional materials and devices. *J. Mater. Chem. C* **2017**, *5*, 12289–12297. [CrossRef]
16. Koswatta, S.O.; Koester, S.J.; Haensch, W. On the Possibility of Obtaining MOSFET-Like Performance and Sub-60-mV/dec Swing in 1-D Broken-Gap Tunnel Transistors. *IEEE Trans. Electron Devices* **2010**, *57*, 3222–3230. [CrossRef]
17. Lei, J.F.; Li, L.B.; Shen, X.H.; Du, K.; Ni, J.; Liu, C.J.; Li, W.S. Fabrication of Ordered ZnO/TiO_2 Heterostructures via a Templating Technique. *Langmuir* **2013**, *29*, 13975–13981. [CrossRef] [PubMed]
18. Ding, M.; Yao, N.; Wang, C.; Huang, J.; Shao, M.; Zhang, S.; Li, P.; Deng, X.; Xu, X. ZnO@CdS Core-Shell Heterostructures: Fabrication, Enhanced Photocatalytic, and Photoelectrochemical Performance. *Nanoscale Res. Lett.* **2016**, *11*, 205. [CrossRef]
19. Verma, S.; Ghosh, H.N. Carrier relaxation dynamics in type-II ZnO/CdSe quantum dot heterostructures. *Phys. Chem. Chem. Phys.* **2017**, *19*, 24896–24902. [CrossRef]
20. Upadhaya, D.; Talinungsang; Kumar, P.; Purkayastha, D.D. Tuning the wettability and photocatalytic efficiency of heterostructure ZnO-SnO_2 composite films with annealing temperature. *Mater. Sci. Semicond. Process.* **2019**, *95*, 28–34. [CrossRef]
21. Wang, L.; Li, J.; Wang, Y.; Yu, K.; Tang, X.; Zhang, Y.; Wang, S.; Wei, C. Construction of 1D SnO_2-coated ZnO nanowire heterojunction for their improved n-butylamine sensing performances. *Sci. Rep.* **2016**, *6*, 35079. [CrossRef]
22. Uddin, T.; Nicolas, Y.; Olivier, C.; Toupance, T.; Servant, L.; Müller, M.M.; Kleebe, H.-J.; Ziegler, J.; Jaegermann, W. Nanostructured SnO_2–ZnO Heterojunction Photocatalysts Showing Enhanced Photocatalytic Activity for the Degradation of Organic Dyes. *Inorg. Chem.* **2012**, *51*, 7764–7773. [CrossRef] [PubMed]
23. Hamrouni, A.; Moussa, N.; Parrino, F.; Di Paola, A.; Houas, A.; Palmisano, L. Sol–gel synthesis and photocatalytic activity of ZnO–SnO_2 nanocomposites. *J. Mol. Catal. A Chem.* **2014**, *390*, 133–141. [CrossRef]
24. Verma, N.; Yadav, S.; Mari, B.; Mittal, A.; Jindal, J. Synthesis and Charcterization of Coupled ZnO/SnO_2 Photocatalysts and Their Activity towards Degradation of Cibacron Red Dye. *Trans. Indian Ceram. Soc.* **2018**, *77*, 1–7. [CrossRef]
25. Nosaka, Y.; Nosaka, A. Understanding Hydroxyl Radical (•OH) Generation Processes in Photocatalysis. *ACS Energy Lett.* **2016**, *1*, 356–359. [CrossRef]
26. Hu, P.; Long, M. Cobalt-catalyzed sulfate radical-based advanced oxidation: A review on heterogeneous catalysts and applications. *Appl. Catal. B Environ.* **2016**, *181*, 103–117. [CrossRef]
27. Wang, N.; Zheng, T.; Zhang, G.; Wang, P. A review on Fenton-like processes for organic wastewater treatment. *J. Environ. Chem. Eng.* **2016**, *4*, 762–787. [CrossRef]
28. Guerra-Rodríguez, S.; Rodríguez, E.; Singh, D.; Rodríguez-Chueca, J. Assessment of Sulfate Radical-Based Advanced Oxidation Processes for Water and Wastewater Treatment: A Review. *Water* **2018**, *10*, 1828. [CrossRef]
29. Yu, B.; Zeng, J.; Gong, L.; Zhang, M.; Zhang, L.; Chen, X. Investigation of the photocatalytic degradation of organochlorine pesticides on a nano-TiO_2 coated film. *Talanta* **2007**, *72*, 1667–1674. [CrossRef]
30. Zheng, L.; Zheng, Y.; Chen, C.; Zhan, Y.; Lin, X.; Zheng, Q.; Wei, K. Facile One-Pot Synthesis of ZnO/SnO_2 Heterojunction Photocatalysts with Excellent Photocatalytic Activity and Photostability. *ChemPlusChem* **2012**, *77*, 217–223. [CrossRef]
31. Huang, X.; Shang, L.; Chen, S.; Xia, J.; Qi, X.; Wang, X.; Zhang, T.; Meng, X. Type-II ZnO nanorod–SnO_2 nanoparticle heterostructures: Characterization of structural, optical and photocatalytic properties. *Nanoscale* **2013**, *5*, 3828–3833. [CrossRef]
32. Zhu, L.; Hong, M.; Ho, G.W. Hierarchical Assembly of SnO_2/ZnO Nanostructures for Enhanced Photocatalytic Performance. *Sci. Rep.* **2015**, *5*, 11609. [CrossRef] [PubMed]

33. Wang, Z.; Gao, S.; Fei, T.; Liu, S.; Zhang, T. Construction of ZnO/SnO_2 Heterostructure on Reduced Graphene Oxide for Enhanced Nitrogen Dioxide Sensitive Performances at Room Temperature. *ACS Sens.* **2019**, *4*, 2048–2057. [CrossRef]
34. Talinungsang; Upadhaya, D.; Kumar, P.; Purkayastha, D.D. Superhydrophilicity of photocatalytic ZnO/SnO_2 heterostructure for self-cleaning applications. *J. Sol-Gel Sci. Technol.* **2019**, *92*, 575–584. [CrossRef]
35. Lu, Z.; Zhou, Q.; Wang, C.; Wei, Z.; Xu, L.; Gui, Y. Electrospun ZnO-SnO_2 Composite Nanofibers and Enhanced Sensing Properties to SF6 Decomposition Byproduct H2S. *Front. Chem.* **2018**, *6*, 540. [CrossRef]
36. Çetinörgü, E.; Goldsmith, S.; Boxman, R.L. Optical properties of transparent ZnO–SnO_2thin films deposited by filtered vacuum arc. *J. Phys. D Appl. Phys.* **2006**, *39*, 1878–1884. [CrossRef]
37. Al-Kandari, H.; Younes, N.; Al-Jamal, O.; Zakaria, Z.Z.; Najjar, H.; Alserr, F.; Pintus, G.; Al-Asmakh, M.A.; Abdullah, A.M.; Nasrallah, G.K. Ecotoxicological Assessment of Thermally- and Hydrogen-Reduced Graphene Oxide/TiO_2 Photocatalytic Nanocomposites Using the Zebrafish Embryo Model. *Nanomaterials* **2019**, *9*, 488. [CrossRef] [PubMed]
38. Athanasekou, C.P.; Moustakas, N.; Morales-Torres, S.; Pastrana-Martínez, L.M.; Figueiredo, J.L.; Faria, J.L.; Silva, A.M.; Rodríguez, J.M.D.; Romanos, G.E.; Falaras, P. Ceramic photocatalytic membranes for water filtration under UV and visible light. *Appl. Catal. B Environ.* **2015**, *178*, 12–19. [CrossRef]
39. Zheng, L.; Zheng, Y.; Chen, C.; Zhan, Y.; Lin, X.; Zheng, Q.; Wei, K.; Zhu, J. Network Structured SnO_2/ZnO Heterojunction Nanocatalyst with High Photocatalytic Activity. *Inorg. Chem.* **2009**, *48*, 1819–1825. [CrossRef]
40. Rogé, V.; Georgantzopoulou, A.; Lenoble, D.; Mehennaoui, K.; Fechete, I.; Garin, F.; Dinia, A.; Gutleb, A.C. Tailoring the optical properties of ZnO nano-layers and their effect on in vitro biocompatibility. *RSC Adv.* **2015**, *5*, 97635–97647. [CrossRef]
41. Wack, S.; Popa, P.L.; Adjeroud, N.; Guillot, J.; Pistillo, B.R.; Leturcq, R. Large-Scale Deposition and Growth Mechanism of Silver Nanoparticles by Plasma-Enhanced Atomic Layer Deposition. *J. Phys. Chem. C* **2019**, *123*, 27196–27206. [CrossRef]
42. Shi, J.; Sun, C.; Starr, M.; Wang, X. Growth of Titanium Dioxide Nanorods in 3D-Confined Spaces. *Nano Lett.* **2011**, *11*, 624–631. [CrossRef] [PubMed]
43. Li, Z.; Wang, R.; Xue, J.; Xing, X.; Yu, C.; Huang, T.; Chu, J.; Wang, K.-L.; Dong, C.; Wei, Z.; et al. Core–Shell ZnO@SnO_2 Nanoparticles for Efficient Inorganic Perovskite Solar Cells. *J. Am. Chem. Soc.* **2019**, *141*, 17610–17616. [CrossRef] [PubMed]
44. Rogé, V.; Lamblin, G.; Fechete, I.; Dinia, A.; Garin, F.; Bahlawane, N.; Lenoble, D. Improvement of the photocatalytic degradation property of atomic layer deposited ZnO thin films: The interplay between film properties and functional performances. *J. Mater. Chem. A* **2015**, *3*, 11453–11461. [CrossRef]
45. Willander, M.; Nur, O.; Sadaf, J.R.; Qadir, M.I.; Zaman, S.; Zainelabdin, A.; Bano, N.; Hussain, I. Luminescence from Zinc Oxide Nanostructures and Polymers and their Hybrid Devices. *Materials* **2010**, *3*, 2643–2667. [CrossRef]
46. Ahn, C.H.; Kim, Y.Y.; Kim, N.C.; Mohanta, S.K.; Cho, H. A comparative analysis of deep level emission in ZnO layers deposited by various methods. *J. Appl. Phys.* **2009**, *105*, 13502. [CrossRef]
47. Matsushima, Y.; Maeda, K.; Suzuki, T. Nature of dark-brown SnO_2 films prepared by a chemical vapor deposition method. *J. Ceram. Soc. Jpn.* **2008**, *116*, 989–993. [CrossRef]
48. Aljawf, R.N.; Alam, M.J.; Rahman, F.; Ahmad, S.; Shahee, A.; Kumar, S. Impact of annealing on the structural and optical properties of ZnO nanoparticles and tracing the formation of clusters via DFT calculation. *Arab. J. Chem.* **2020**, *13*, 2207–2218. [CrossRef]
49. Gultekin, I.; Ince, N.H. Degradation of reactive azo dyes by UV/H2O2: Impact of radical scavengers. *J. Environ. Sci. Health Part A* **2004**, *39*, 1069–1081. [CrossRef]
50. Oluwabi, A.T.; Gaspar, D.; Katerski, A.; Mere, A.; Krunks, M.; Pereira, L.; Acik, I.O. Influence of Post-UV/Ozone Treatment of Ultrasonic-Sprayed Zirconium Oxide Dielectric Films for a Low-Temperature Oxide Thin Film Transistor. *Materials* **2019**, *13*, 6. [CrossRef]
51. Shi, S.; Li, J.; Bu, T.; Yang, S.; Xiao, J.; Peng, Y.; Li, W.; Zhong, J.; Ku, Z.; Cheng, Y.-B.; et al. Room-temperature synthesized SnO_2 electron transport layers for efficient perovskite solar cells. *RSC Adv.* **2019**, *9*, 9946–9950. [CrossRef]
52. Yi, Z.; Wang, J.; Jiang, T.; Tang, Q.; Cheng, Y. Photocatalytic degradation of sulfamethazine in aqueous solution using ZnO with different morphologies. *R. Soc. Open Sci.* **2018**, *5*, 171457. [CrossRef] [PubMed]

53. Zhang, Q.; Xu, M.; You, B.; Zhang, Q.; Yuan, H.; Ostrikov, K. (Ken) Oxygen Vacancy-Mediated ZnO Nanoparticle Photocatalyst for Degradation of Methylene Blue. *Appl. Sci.* **2018**, *8*, 353. [CrossRef]
54. Lin, J.; Luo, Z.; Liu, J.; Li, P. Photocatalytic degradation of methylene blue in aqueous solution by using ZnO-SnO_2 nanocomposites. *Mater. Sci. Semicond. Process.* **2018**, *87*, 24–31. [CrossRef]
55. Hou, C.; Hu, B.; Zhu, J. Photocatalytic Degradation of Methylene Blue over TiO_2 Pretreated with Varying Concentrations of NaOH. *Catalysts* **2018**, *8*, 575. [CrossRef]
56. Zhang, H.; Han, Y.; Yang, L.; Guo, X.; Wu, H.; Mao, N. Photocatalytic Activities of PET Filaments Deposited with N-Doped TiO_2 Nanoparticles Sensitized with Disperse Blue Dyes. *Catalysts* **2020**, *10*, 531. [CrossRef]